Atmos. Chem. Phys., 23, 7213–7223, 2023
https://doi.org/10.5194/acp-23-7213-2023

Atmospheric Chemistry and Physics
Open Access
EGU

Measurement report: Atmospheric aging of combustion-derived particles – impact on stable free radical concentration and its ability to produce reactive oxygen species in aqueous media

Heather L. Runberg and Brian J. Majestic

Department of Chemistry and Biochemistry, University of Denver, Denver, CO 80208-9020, USA

Correspondence: Brian J. Majestic (brian.majestic@du.edu)

Received: 10 January 2023 – Discussion started: 30 January 2023
Revised: 23 May 2023 – Accepted: 25 May 2023 – Published: 30 June 2023

Abstract. Environmentally persistent free radicals (EPFRs) are a pollutant found on fine atmospheric particulate matter ($PM_{2.5}$), particularly on $PM_{2.5}$ formed from combustion processes. EPFRs are organic radicals that can endure in the environment for days to years. Interest in the toxicity of EPFRs has increased significantly in recent years, as it has been shown to have substantial ability to form reactive oxygen species (ROS), but little is known about how its characteristics change as $PM_{2.5}$ ages in the atmosphere. Here, we exposed newly produced hexane-generated soot to simulated sunlight for 24 h. Changes to the EPFR characteristics of the particles were measured by electron paramagnetic resonance (EPR) spectroscopy. The soot was then added to water, and a second exposure to light was used to measure hydroxyl radical (OH) formation from both photoaged and dark-aged soot. There were no changes to EPFR characteristics (spin concentration, g factor, peak width, or lineshape) due to the exposure to simulated sunlight; however, the soot's ability to form OH was greatly reduced by photoaging. Photoaged soot resulted in an almost 60 % reduction in OH formation over soot which had been aged in the dark for the same amount of time.

1 Introduction

Fine atmospheric particulate matter, particles smaller than 2.5 µm in diameter ($PM_{2.5}$), is a well-documented environmental problem. Because of their small size, $PM_{2.5}$ can penetrate deep into the lungs where it has been shown to cause oxidative damage via the production of reactive oxygen species (ROS) (Feng et al., 2016; Vidrio et al., 2009). $PM_{2.5}$ has been linked to many cardiopulmonary health concerns such as asthma, high blood pressure, and chronic obstructive pulmonary disease (COPD) (He et al., 2022; Chan et al., 2008), as well as diabetes (Brook et al., 2012, 2013) and cancer (Guo et al., 2020; Katanoda et al., 2011). One of the major sources of $PM_{2.5}$ is combustion, from sources such as automobile exhaust, power plants, and wildfires. Climate change has already driven an increase in the number and severity of wildfires globally (Coop et al., 2022), and there is evidence that $PM_{2.5}$ from wildfires may be more hazardous than from other sources (Aguilera et al., 2021).

$PM_{2.5}$ can stay aloft for a very long time and can travel thousands of kilometers from its point source. During this time, it is subjected to various environmental conditions such as weather, sunlight, and interaction with atmospheric gases like NO_x, SO_x, or reactive oxygen species (ROS, e.g., OH, O_3, O^{2-}), all of which can alter the chemical composition of $PM_{2.5}$ components, resulting in aging of the particles (Liu and Chan, 2022; Donahue et al., 2009).

Additionally, $PM_{2.5}$ has been shown to contain substantial concentrations of environmentally persistent free radicals (EPFRs) (Chen et al., 2018; Runberg et al., 2020), a newly identified class of pollutant. Radicals are chemical species with at least one unpaired electron and typically are very reactive, with lifetimes generally on the scale of nanoseconds. EPFRs, however, persist for days, weeks, or even years in

the environment making them an important environmental contaminant (Gehling and Dellinger, 2013). EPFRs are generally carbon- and oxygen-centered radicals and have been shown to form from the same combustion systems that result in $PM_{2.5}$ (Wang et al., 2019). Both $PM_{2.5}$ and EPFRs have been reported to induce ROS formation (Tong et al., 2018; Arangio et al., 2016; Khachatryan et al., 2011), and it is possible that the EPFR component is a significant contributor of $PM_{2.5}$'s ability to form ROS.

To date, little is known about the impacts of atmospheric aging on EPFRs bound to $PM_{2.5}$, such as its character, concentrations, or its ability to mediate ROS formation. One of the key components of $PM_{2.5}$ is soot, which contains EPFRs, and as such it was chosen as a surrogate for environmental PM because its age and environmental encounters could be controlled.

In this study, the EPFR characteristics of fresh hexane-derived soot are compared to soot that has been photoaged. EPFR concentrations and characteristics are measured by electron paramagnetic resonance (EPR) spectroscopy, Fourier-transform infrared (FT-IR) spectroscopy, and gas chromatography mass spectrometry (GC-MS) before and after illumination under a solar simulator. Additionally, the ability of both the photoaged and non-aged soot to produce OH in aqueous media is studied, and the EPFR characteristics of the soot after OH formation are also investigated.

2 Materials and methods

2.1 Photoaging of combustion particles

2.1.1 Stage I

Hexane-derived soot was produced as previously described (Runberg et al., 2020) by using a diffusion flame with a glass funnel inverted above the flame to accumulate the soot. The soot was collected from the funnel into a disposable aluminum baking dish (Reynolds KITCHENS® mini loaf pan) as soon as it was cool (Fig. 1-I). The soot was transferred to the aluminum baking dishes only after it was fully cooled to prevent any interference from the foil on the EPFR structure.

2.1.2 Stage II

The bulk soot was divided roughly evenly between two additional baking dishes. One dish was placed under a xenon lamp solar simulator (Oriel Sol 1A, Newport Solar Simulator equipped with an AM 1.5 Global filter) calibrated to one sun at the average North American zenith, and the other was kept in the dark by covering it with aluminum foil. The soot was aged in this manner for 24 h (Fig. 1-II). This process was completed twice: once to produce soot for photoreactions in stage III, which included an OH probe, and once for reactions executed without an OH probe.

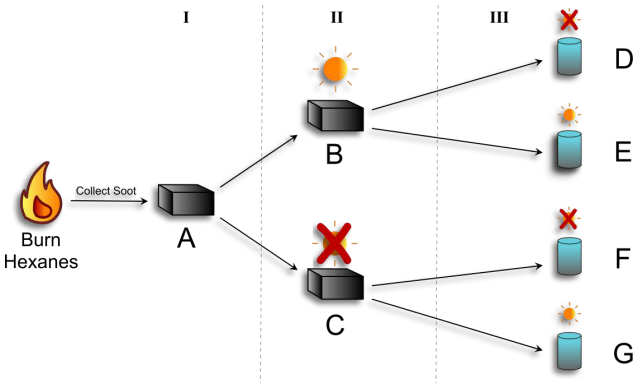

Figure 1. Schematic of photoaging experimental setup. Hexanes were burned and resultant soot was collected (A). That soot was divided: half was exposed to simulated sunlight for 24 h (B), and half was kept in the dark (C). The soot from each was then added to water to make a slurry. The two soot slurries were then divided in half: and one was exposed to simulated sunlight for 16 h (E and G), and the other was kept in the dark (D and F). Soot characterization was done at each stage (I, II, and III), via GC-MS, FT-IR, and EPR. OH production was measured for stage III.

2.1.3 Stage III

After the soot had been aged for 24 h, either with or without light, it was combined with ultra-pure water (18 MΩ) (Fig. 1-III) and stirred overnight to create a well-mixed suspension, or slurry. Using a microbalance, 0.0225 ± 0.0005 g of soot was combined with 500 mL of Milli-Q water for a final soot concentration of 45 ± 0.5 ppm (m/v) for slurries that were used for OH measurements. This is in line with concentrations of $PM_{2.5}$ obtained in previous work (Leresche et al., 2021). For slurries used for all other analyses, 118 ± 2 ppm (m/v) was used. Slurry concentrations for non-OH analyses were higher to allow for enough soot to be collected after the photoreactions for EPFR, FT-IR, and GC-MS analysis.

Samples of the prepared slurries were poured into two Teflon reaction vessels for the aqueous reaction in Stage III. Both reaction vessels were placed into water-cooled, jacketed glass beakers which were kept at 25 °C. One was located under the solar simulator, and the other was covered with aluminum foil to keep it dark. The slurries were stirred continuously for the 16 h reaction time. For EPFR, FT-IR, and GC-MS analyses, the reactants were poured into clean baking dishes and dried overnight in an oven set to 50 °C. Once the soot was dry, it was collected for further analysis. All samples were stored in a freezer when not being analyzed, with storage times ranging from two to seven days (Table A1).

2.2 EPR analysis

Samples of soot ranging between $0.4–0.9 \pm 0.1$ mg were collected in triplicate in 1.5 mm ID Pyrex closed-bottom capil-

lary tubes after each stage of photoaging for later EPR investigation; samples were capped with Critoseal and stored in a freezer until analysis. EPR analysis and EPFR characterization of soot samples were performed using previously described methods (Runberg et al., 2020). EPFR concentrations were measured using the spin-count feature available in the Bruker EMXnano Xenon software (see Table A1 for Q values and frequencies obtained). Spin counts were determined in triplicate for each sample and averaged. Lineshape evaluation, including g factors and Gaussian and Lorentzian line contributions, was performed using least squares analysis available in the EasySpin package (version 5.2.35) (Stoll and Schweiger, 2006) available in MATLAB (Table A1). Triplicate soot samples were averaged together for final lineshape analysis.

2.3 Determination of [OH] via HPLC

Sodium benzoate (SBA) was used as an OH probe because it readily forms *para*-hydroxybenzoic acid (*p*-HBA) when exposed to OH radicals (Wu et al., 2017); *p*-HBA is relatively stable and can be easily quantified via high-performance liquid chromatography (HPLC). SBA (1.0 mM) was added to 45 ppm soot slurries just prior to beginning the photoreaction. This concentration was selected to be in substantial excess of the expected OH concentration, allowing the probe to capture the majority of the OH formed during the reaction. Aliquots of approximately 5 mL of soot slurry were collected before and after 16 h photoreactions and filtered using 0.2 µm, 25 mm diameter Whatman polypropylene filters. Filters were rinsed with a minimum of 15 mL ultrapure water prior to filtering. Filtrate was analyzed with no further modification via HPLC (Agilent 1100 with diode-array detector (DAD) and a C-18 Hydro-RP 250 × 4.6 mm column, Phenomenex) using the method described previously (Runberg and Majestic, 2022). Each sample was run in triplicate, and final *p*-HBA concentrations were averaged.

Fresh *p*-HBA standards were prepared in ultrapure water on the day of analysis, with a limit of quantification of 0.11 ± 0.06 µM, as determined by dividing the standard deviation of the response by the slope of the calibration curve and multiplying by 10 (Borman and Elder, 2017). Total OH production during the course of the reaction was determined by dividing the measured *p*-HBA concentration by the fraction of OH that forms *p*-HBA after 16 h, previously determined to be 0.56 (Runberg and Majestic, 2022).

2.4 GC-MS analysis

A solid–liquid organic extraction was done to obtain the organic-soluble fraction of soot for analysis via gas chromatography mass spectroscopy (GC-MS). Soot from each stage of the photoaging process was extracted into acetonitrile (ACN) by submerging a small amount into an aliquot of ACN and allowing it to soak overnight. The ACN was then filtered using a 0.2 µm polypropylene Whatman filter to remove any remaining soot particulate before examination via an Agilent 7820A GC system coupled to a 5977B MSD. A previously described GC-MS method was used (Runberg and Majestic, 2022), and mass spectral analysis was preformed using Agilent MassHunter Qualitative Analysis Navigator (B.08.00) and NIST MS Search (version 2.3).

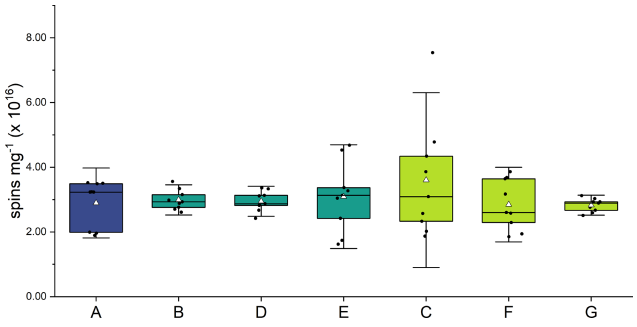

Figure 2. EPFR concentrations (spins per mg of soot) from soot samples at each step of the aging process (A–G). Three soot samples were collected from each phase of the experiment, and spins were calculated in triplicate for each sample. Average is shown as a white triangle.

2.5 FT-IR

Fourier-transform infrared spectroscopy (FTIR) was done for all samples to assess any bulk changes to functional groups as the soot is aged. The system used was a D5 ATR Diamond Thermo Fisher Scientific spectrograph. Analysis was performed by doing 30 scans per sample.

3 Results

3.1 EPFR characterization

Figure 2 and Table A1 present the EPFR concentrations at various stages in the aging process. There was no significant difference in EPFR concentration at any phase of the soot aging process. Concentrations of EPFRs ranged from (2.5 ± 0.3) to $(3.4 \pm 0.6) \times 10^{16}$ spins mg^{1}. These concentrations are consistent with previous soot and biochar studies (Runberg et al., 2020; Tian et al., 2009; Sigmund et al., 2021).

One way to characterize an EPR signal is by determining the associated g factor, a unitless proportionality constant determined by the ratio of the magnetic field and the applied microwave frequency. Equation (1) shows the relationship of g to the frequency (υ) and the magnetic field (B), where h is Planck's constant and β is the Bohr magnetron (Eaton et al., 2010); see Eq. (1):

$$g = \frac{h\upsilon}{\beta B}. \quad (1)$$

Electrons are half-spin particles with two possible spin states, $+1/2$ and $-1/2$, with the difference in energy between them equal to ΔE. In EPR spectroscopy, the microwave frequency (ν) is usually held constant while the magnetic field (B) is modulated. When ΔE equals the applied microwave energy, resonance is achieved and absorption occurs, resulting in an EPR signal. The g factor at the point of resonance can be used to identify the type of radical being measured (Eaton et al., 2010; EPR-Interpretation, 2022).

In the current study, there were no changes observed to the g factor of the soot over the course of the aging process, which was between 2.0056–2.0057 for all samples (Table A1 and Fig. A1) and is consistent with the g factor of an organic radical (EPR-Interpretation, 2022). Because of the lack of hyperfine splitting in the EPR signal, it can be deduced that the soot is comprised of a large number of organic radicals which cannot be uniquely defined. Changes in g factor indicate a change in radical type, for example, a shift from predominantly carbon-centered to predominantly oxygen-centered radicals, which was not observed in this study. However, this g factor is notably higher than those reported in our previous study (Runberg et al., 2020), which were 2.0028 ± 0.0001. The soot for both studies was obtained in an identical manner, but the current study appears to have a much higher concentration of oxygen- or nitrogen-centered radicals. This is likely due to the use of a diffusion flame, which cannot control the air-to-fuel ratio, and oxygen or nitrogen was likely incorporated during combustion. While it is outside the scope of this study, it would be useful to control for this factor in future investigations.

A second parameter that can be used to characterize an EPFR signal is its peak width ($\Delta B_{\mathrm{p-p}}$), measured as the distance along the x axis (magnetic field, B) between the maximum and minimum absorbances (peaks) of the derivative EPR signal. Both the peak width and the lineshape (discussed below) provide information about how the varying spin environments in a complex sample interact with one another. Changes to $\Delta B_{\mathrm{p-p}}$ indicate changes to the composition of the bulk sample (Sorin and Vlasova, 1973).

There was no difference in peak width between any of the dry samples (fresh, photoaged, and dark-aged), indicating no impact to the spin environments from the photoaging of dry soot. However, there were small but statistically significant differences between the dry and the wetted samples (t tests done at 95 % certainty, with $p < 0.05$) (Fig. 3). The $\Delta B_{\mathrm{p-p}}$ decreased for both aged soot samples (dark and light) upon submersion and agitation in water. For soot that had been photoaged dry, $\Delta B_{\mathrm{p-p}}$ decreased 4.4 % in the dark and 5.7 % when exposed to light. For soot that had been dark-aged dry, $\Delta B_{\mathrm{p-p}}$ decreased 5.2 % in the dark and 5.8 % when exposed to light. Additionally, when comparing the peak width of the wetted soot samples, soot that had been kept in the dark for dry-aging had $\Delta B_{\mathrm{p-p}}$ 2.3 % smaller than soot that had been dry-aged in light. This decrease in $\Delta B_{\mathrm{p-p}}$ is likely an artifact of the increase in Gaussian character of the spectral lines for

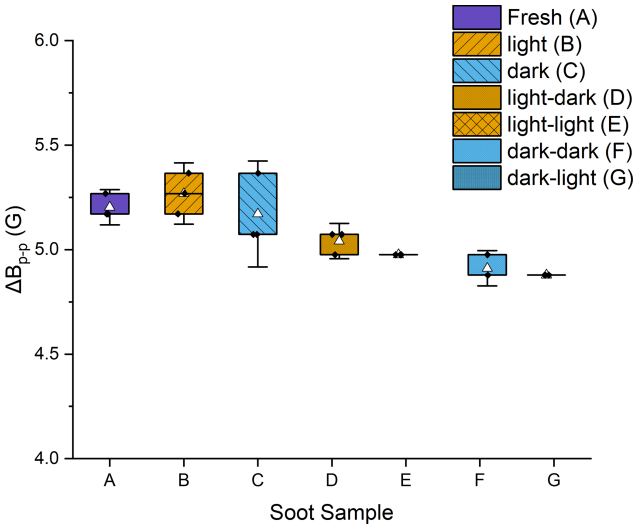

Figure 3. Box plot of peak-to-peak widths ($\Delta B_{\mathrm{p-p}}$) for each of the soot stages. Error bars are the standard deviation of three trials. The average is shown as a white triangle. Samples A, B, and C were dry soot; samples D–G had been wetted and then dried prior to analysis.

samples that had been submerged and agitated in water. This is discussed further in the next section.

Lineshape is another way to characterize an EPFR signal. EPR lines are complex functions comprised of the signals from each unpaired electron in the bulk sample. The bulk signal is modeled as a summation of each individual signal, using Gaussian and Lorentzian line functions. The more homogenous the sample, the more Lorentzian in character the lineshape will be. A more complex sample will result in more hyperfine coupling, which results in an increase in Gaussian character (Petrakis, 1967).

In this study, EPR lineshapes were seen to change in the wet portion of the aging process, with a significant decrease in Lorentzian character and an increase in Gaussian character (Fig. 4) indicating a decrease in the homogeneity of the EPFR environments in the soot and an increase in hyperfine interactions. Gaussian contribution increased from an average of (0.06 ± 0.03) mT across stages I and II to (0.22 ± 0.01) mT in stage III, an increase of 133 %. Lorentzian contribution decreased 17 % from a combined average of (0.51 ± 0.02) mT for dry soot to (0.40 ± 0.01) mT wetted soot. This is an indication that the variability of electron environments within the sample increased with exposure to the water, but not to the light. This is counter to our previous study which did not result in any lineshape changes due to exposure to water. However, in that study, the soot was submerged and not agitated. So, the lineshape change seen here is likely due to the continuous agitation that occurred during the photoreaction, which broke up large soot fragments. An increase in soot density was observed between dry soot and soot that had been wetted (see Table A1), supporting this assessment. Soot density was determined by dividing

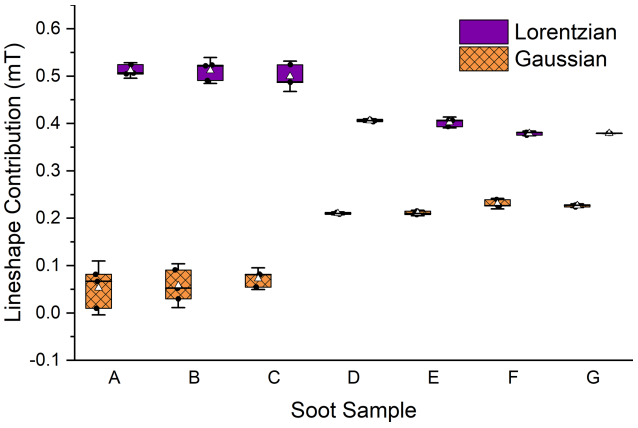

Figure 4. Changes in Gaussian and Lorentzian contributions to the EPR lineshape. Error bars are the standard deviation of three trials. The average is shown as a white triangle. Samples A, B, and C were dry soot; samples D–G had been wetted and then dried prior to analysis.

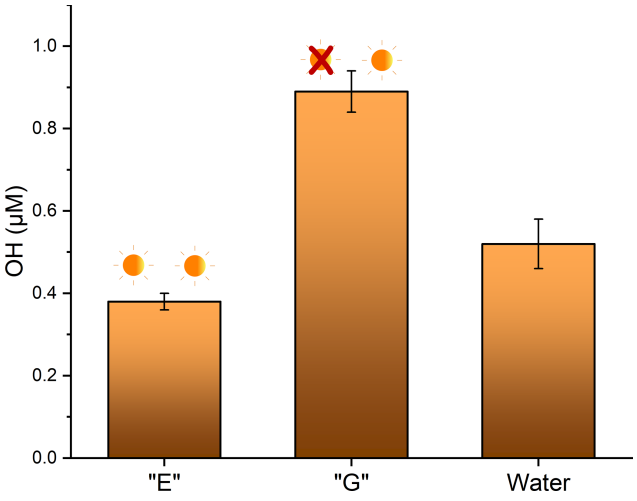

Figure 5. Production of OH measured after 16 h lighted reactions of soot that had been previously aged for 24 h in the light (E), aged for 24 h in the dark (G), and an ultrapure water control.

the mass of the soot by the height of the soot in the capillary tube.

3.2 Hydroxyl radical (OH) formation

The ability of soot to produce OH was measured in aqueous conditions to mimic the conditions in a droplet of cloud water. Analysis was separated by soot that had been previously photoaged and soot that had been previously aged in the dark. No measurable OH was observed in either of the dark reactions (Fig. 1, samples D and F), confirming that light is required for OH production. For soot slurries that were exposed to light, soot that had been photoaged for 24 h previously had the lowest OH production at 0.38 ± 0.02 µM. This is not significantly different ($p = 0.06$) than controls done in ultrapure water, which were (0.52 ± 0.06) µM. Soot that had been dark-aged for 24 h prior to the photoreaction in water resulted in significantly higher OH production, at (0.89 ± 0.05) µM (Fig. 5) ($p < 0.005$). This is consistent with a recent study reporting a decrease in OH formation in wildfire smoke plumes downfield from the point source vs. the same plume measured nearer to the source (Akherati et al., 2022). This indicates that smoke which has been exposed to sunlight for a longer period of time (i.e., the downfield plume) results in lower OH production. While photoaging of airborne soot particles in a much more complex system such as a smoke plume is likely not the only reason for the decline (e.g., there are multiple OH production pathways and the plume is diluted), the same pattern of diminished OH production is reported. A laboratory study showed reduced ROS activity in aged PM as well (Gehling et al., 2014). In that study, particulate matter was aged at room temperature in phosphate buffered saline solution to maintain a physiologically neutral pH, but no application of light was executed. The authors reported a decrease OH formation of about 11 % after 1 d. This implies that other factors may play a role in the aging of soot, in addition to sunlight.

3.3 GC-MS

GC-MS analysis was done to qualitatively determine if there was a change in the number of organic-soluble compounds in the soot at different stages of the aging process. In all dry soot samples (samples A, B, and C in Fig. 1), only one compound was seen, at a retention time of 9.13 min (Fig. 6a and b). Analysis of the fragmentation pattern of this peak indicated no obvious nitrogen- or oxygen-containing fragments. For all samples that had been submerged in water (samples D–G in Fig. 1), there were several new peaks observed (Fig. 6, middle and bottom rows). Mass spectral comparisons to the NIST MS database did not definitively identify any of the compounds, but all display a distinctly hydrocarbon-like fragmentation pattern (Fig. A2).

There is indication that oxygen is being incorporated into the new peaks observed in samples that had been wetted. For example, analysis of the fragmentation pattern on the peak which eluted at 13.44 min suggests a McLafferty rearrangement (Burgers and Terlouw, 2016), resulting in an acylium cation with $m/z = 43$ and a McLafferty fragment at $m/z = 57$, implying the presence of at least one carbonyl group (Fig. A3).

3.4 Fourier transform infrared (FTIR) spectroscopy

Fourier transform infrared (FTIR) spectroscopy was done for all soot samples to assess bulk changes in functional groups. All dry soot samples appear nearly identical, indicating no changes to functionality via dry aging. There is new peak

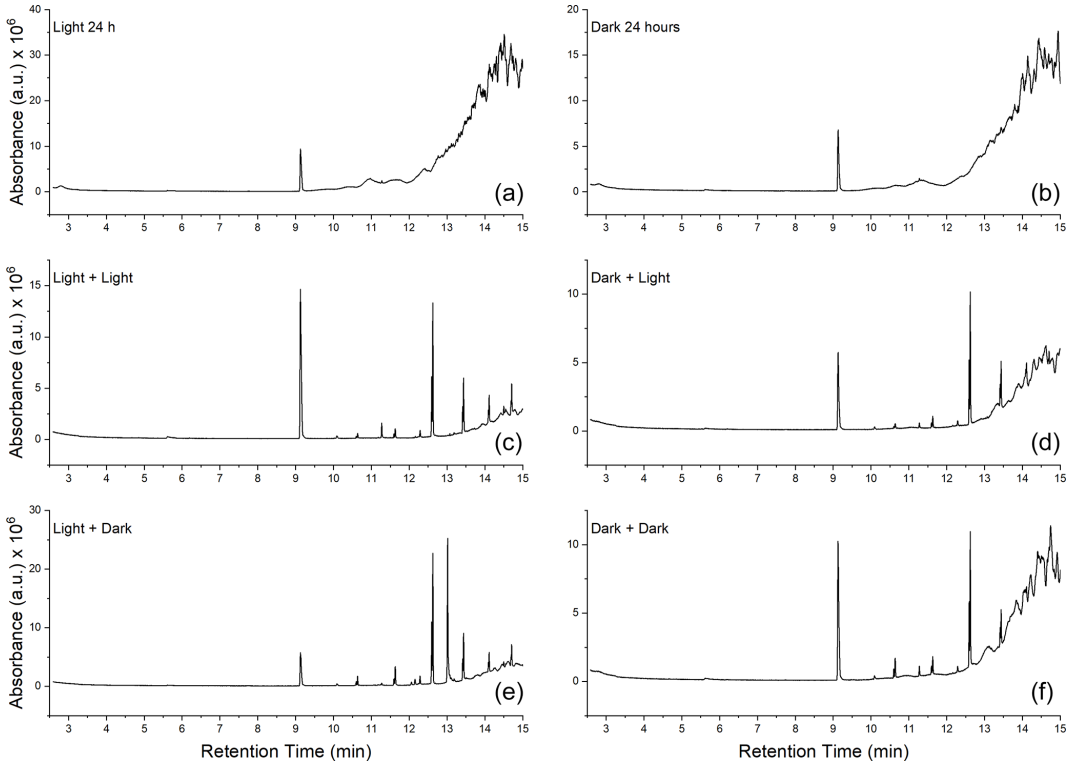

Figure 6. Gas chromatograms of soot at each step of the aging process. **(a, c, e)** Chromatograms of soot extracts taken from the photoaged pathway (samples B → E and D). **(b, d, f)** Extracts of soot that followed the dark-aged pathway (samples C → G and F). **(a, b)** Extracts from the soot after initial 24 h of aging. **(c, d)** Soot that was photoaged in water for 16 h. **(e, f)** Soot that was dark aged in water for 16 h.

formation in all samples that had been wetted, indicating that the change is likely due to the prolonged agitation in water rather than due to photoreactions of the soot or with any OH formed during the reaction. New peaks were observed at about 2915 and 2850 cm^{-1}, consistent with an increase in C–H stretch, and at 1207 and 1140 cm^{-1}, which indicate a C–O stretch (Fig. 7). Additionally, several peaks are observed in all samples: a peak at 1575 cm^{-1} suggests the presence of N–O stretching, a peak at 1730 cm^{-1} may be C = N, and a peak at 2090 cm^{-1} may be C = C = N, offering evidence of the nitro-components suggested by the g factor of this soot, and was likely introduced during the combustion process.

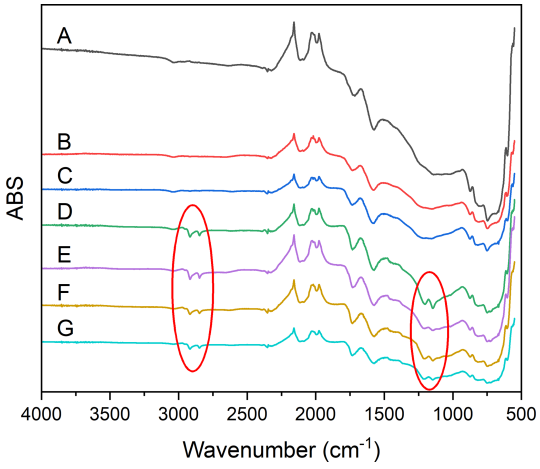

Figure 7. FTIR spectra of all soot samples. Fresh soot (A), dry soot after 24 h of illumination (B), dry soot after 24 h in the dark (C), soot that was photoaged for 24 h, followed by 16 h in the dark, in water (D), soot that was photoaged for 24 h, followed by 16 h in the light, in water, soot that was dark-aged for 24 h, followed by 16 h in the dark, in water (F), soot that was dark-aged for 24 h, followed by 16 h in the light in water (G). Red circles indicate new peaks associated with incorporation of oxygen.

4 Conclusions

EPFR characteristics of combustion particles, such as g factor, lineshape, peak width, and spin concentration, are unaffected by photoaging; however, soot's ability to generate OH when exposed to sunlight diminishes drastically after light exposure. This implies several possibilities: first, it may be something other than EPFRs within the particles that drives the OH formation or, second, that only EPFRs on the surface of the particles are available for OH formation, while the bulk of the EPFR component is bound within the particles where they are not impacted by the light. Combustion par-

ticles that were not photoaged produced almost 60 % more OH than photoaged soot did. It is possible that any changes to the surface EPFRs due to exposure to light were muted by the larger concentration of EPFRs found within the particles, resulting in no meaningful change to the EPFR concentration or characteristics of the exposed soot. The lack of changes to chemical composition of the soot upon irradiation, as seen in the GC-MS and UV–Vis analysis, supports the hypothesis that only EPFRs on the surface of the particle are available for OH formation.

Other environmental factors – specifically the chemical composition of natural cloud waters – may impact the way that combustion particles age in the environment, including some properties of EPFRs, and future work should include this variable. Natural cloud waters are a complex matrix containing compounds such as sulfates, nitrates, metals, and organic matter. Previous work has indicated that natural cloud water has a much lower pH than pure water, and the lower pH of natural cloud water has been implicated in increased solubility of organic aerosols (Li et al., 2020), which may influence photoinduced OH formation from soot.

In summary, EPFR characteristics of soot do not change upon photoaging, but the soot's ability to generate OH is greatly reduced. This has implications to human health, because it implies that freshly generated soot, as from a wildfire, is potentially more hazardous upon inhalation than is soot that has traveled further away from its point source. This could result in an increase in negative health outcomes for people living close to frequent wildfires. Due to global climate change, the frequency and intensity of wildfires is expected to increase, which means that more people will become exposed to freshly generated soot particles. Future studies should investigate the differences in EPFR characteristics and OH production using multiple fuel sources, including biofuels such as seen in wildfires.

Appendix A

Table A1. EPR data for each soot sample collected. Samples were collected in triplicate from each batch.

Batch	Q value	Frequency (GHz)	g factor	Gaussian (mT)	Lorentzian (mT)	Soot density (mg mm^{-1})	Spins mg^{-1}		Freezer storage (days)
A:	4105	9.659	2.0057	0.0817	0.5066	0.052	3.24×10^{16}	$\pm 1.26 \times 10^{14}$	7
Fresh soot	4104	9.658	2.0055	0.0668	0.5046	0.056	3.50×10^{16}	$\pm 3.48 \times 10^{14}$	7
	4105	9.659	2.0056	0.0099	0.5244	0.104	1.95×10^{16}	$\pm 1.58 \times 10^{15}$	7
B:	4105	9.659	2.0055	0.0523	0.5232	0.076	2.93×10^{16}	$\pm 2.00 \times 10^{14}$	6
Dry photoaged	3518	9.658	2.0056	0.0907	0.4908	0.086	3.16×10^{16}	$\pm 2.65 \times 10^{14}$	6
soot	4105	9.659	2.0056	0.0299	0.5216	0.081	2.85×10^{16}	$\pm 4.16 \times 10^{15}$	6
C:	4104	9.659	2.0057	0.0818	0.4877	0.108	2.57×10^{16}	$\pm 2.89 \times 10^{14}$	6
Dry dark-aged	4104	9.657	2.0057	0.0808	0.4867	0.100	3.11×10^{16}	$\pm 1.52 \times 10^{16}$	6
soot	3518	9.659	2.0056	0.0548	0.5242	0.067	4.36×10^{16}	$\pm 1.72 \times 10^{15}$	6
F:	4105	9.660	2.0056	0.2084	0.4089	0.161	3.13×10^{16}	$\pm 7.81 \times 10^{14}$	2
Dark-aged soot,	4105	9.660	2.0055	0.2123	0.4059	0.180	2.87×10^{16}	$\pm 2.08 \times 10^{14}$	2
dark OH	3519	9.660	2.0056	0.2100	0.4039	0.178	2.82×10^{16}	$\pm 1.13 \times 10^{15}$	2
G:	4105	9.659	2.0056	0.2152	0.3934	0.200	2.42×10^{16}	$\pm 2.00 \times 10^{14}$	2
Dark-aged soot,	4105	9.660	2.0056	0.2101	0.4062	0.167	3.37×10^{16}	$\pm 1.15 \times 10^{15}$	2
light OH	4105	9.660	2.0056	0.2078	0.4073	0.180	3.03×10^{16}	$\pm 1.65 \times 10^{15}$	2
D:	4105	9.659	2.0055	0.2393	0.3754	0.220	2.58×10^{16}	$\pm 7.21 \times 10^{14}$	2
Photoaged soot,	3518	9.659	2.0056	0.2266	0.3809	0.236	2.29×10^{16}	$\pm 5.96 \times 10^{15}$	2
dark OH	4105	9.659	2.0056	0.2262	0.3813	0.244	2.72×10^{16}	$\pm 1.08 \times 10^{15}$	2
E:	3519	9.661	2.0056	0.2238	0.3790	0.193	2.93×10^{16}	$\pm 5.48 \times 10^{15}$	2
Photoaged soot,	3518	9.660	2.0056	0.2288	0.3792	0.207	2.92×10^{16}	$\pm 3.46 \times 10^{14}$	2
light OH	3518	9.658	2.0056	0.2274	0.3794	0.227	2.61×10^{16}	$\pm 7.64 \times 10^{15}$	2

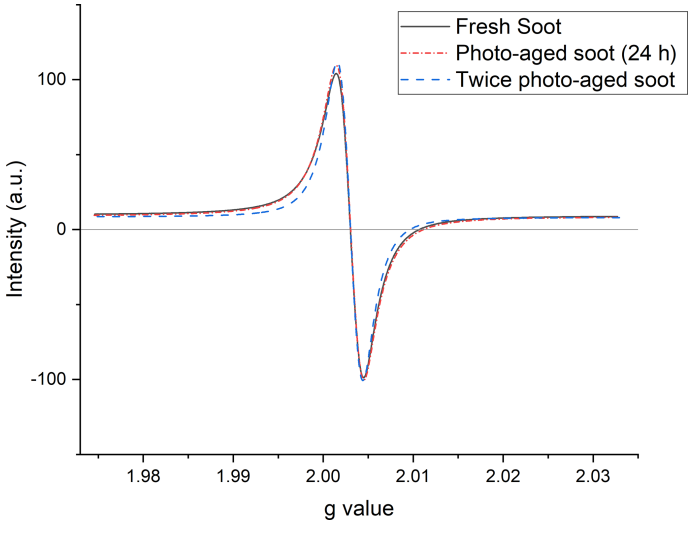

Figure A1. Representative EPR spectra of three soot samples at different stages of photoaging: fresh (black, solid line); soot aged for 24 h under simulated sunlight (red dash–dot); and soot photoaged twice, once dry, and once wet (blue, dash–dash). Signals have been baseline corrected and intensity normalized.

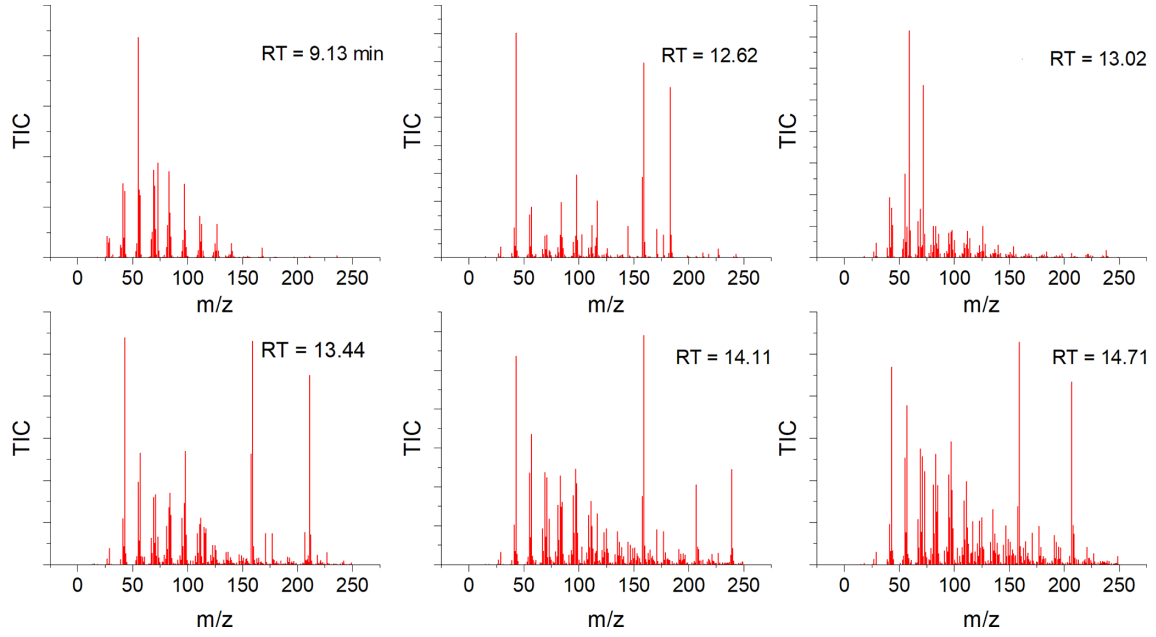

Figure A2. Mass spectra of select peaks from the GC obtained from "light → dark" soot extracted into acetonitrile. Retention times refer to those seen in Fig. 6.

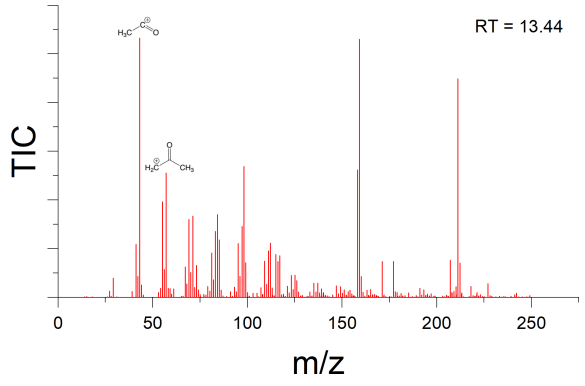

Figure A3. Mass spectrum of the peak seen at retention time 13.44 min.

Data availability. Data described in this article can be accessed at the following repository: https://doi.org/10.56902/Chem.Data.2023.1 (Majestic and Runberg, 2023).

Author contributions. HLR: methodology, software, validation, investigation, writing – original draft, data curation, visualization BJM: conceptualization, resources, writing – review and editing, supervision, project administration.

Competing interests. The contact author has declared that neither of the authors has any competing interests.

Disclaimer. Publisher's note: Copernicus Publications remains neutral with regard to jurisdictional claims in published maps and institutional affiliations.

Acknowledgements. The authors thank Sandra and Gareth Eaton at the University of Denver for allowing us access to their lab's EMX Nano for this research, as well as for their expertise and assistance in analyzing EPR spectra.

Review statement. This paper was edited by Thomas Berkemeier and reviewed by Guorui Liu and Xiao-San Luo.

References

Aguilera, R., Corringham, T., Gershunov, A., and Benmarhnia, T.: Wildfire smoke impacts respiratory health more than fine particles from other sources: observational evidence from Southern California, Nat. Commun., 12, 1493, https://doi.org/10.1038/s41467-021-21708-0, 2021.

Akherati, A., He, Y., Garofalo, L. A., Hodshire, A. L., Farmer, D. K., Kreidenweis, S. M., Permar, W., Hu, L., Fischer, E. V., Jen, C. N., Goldstein, A. H., Levin, E. J. T., DeMott, P. J., Campos, T. L., Flocke, F., Reeves, J. M., Toohey, D. W., Pierce, J. R., and Jathar, S. H.: Dilution and photooxidation driven processes explain the evolution of organic aerosol in wildfire plumes, Environmental Science: Atmospheres, 2, 1000–1022, https://doi.org/10.1039/D1EA00082A, 2022.

Arangio, A. M., Tong, H., Socorro, J., Pöschl, U., and Shiraiwa, M.: Quantification of environmentally persistent free radicals and reactive oxygen species in atmospheric aerosol particles, Atmos.

Chem. Phys., 16, 13105–13119, https://doi.org/10.5194/acp-16-13105-2016, 2016.

Borman, P. and Elder, D.: Q2(R1) Validation of Analytical Procedures, in: ICH Quality Guidelines, John Wiley & Sons, Ltd, 127–166, https://doi.org/10.1002/9781118971147.ch5, 2017.

Brook, R. D., Xu, X., Bard, R. L., Dvonch, J. T., Morishita, M., Kaciroti, N., Sun, Q., Harkema, J., and Rajagopalan, S.: Reduced metabolic insulin sensitivity following sub-acute exposures to low levels of ambient fine particulate matter air pollution, Sci. Total Environ., 448, 66–71, https://doi.org/10.1016/j.scitotenv.2012.07.034, 2012.

Brook, R. D., Cakmak, S., Turner, M. C., Brook, J. R., Crouse, D. L., Peters, P. A., Van Donkelaar, A., Villeneuve, P. J., Brion, O., Jerrett, M., Martin, R. V, Rajagopalan, S., Goldberg, M. S., Arden, C., and Burnett, R. T.: Long-Term Fine Particulate Matter Exposure and Mortality From Diabetes in Canada, Diabetes Care, 36, 3313–3320, https://doi.org/10.2337/dc12-2189, 2013.

Burgers, P. C. and Terlouw, J. K.: Ion structures in mass spectrometry, in: Encyclopedia of Spectroscopy and Spectrometry, Elsevier, 322–329, https://doi.org/10.1016/B978-0-12-803224-4.00182-5, 2016.

Chan, C.-C., Chuang, K.-J., Chen, W.-J., Chang, W.-T., Lee, C.-T., and Peng, C.-M.: Increasing cardiopulmonary emergency visits by long-range transported Asian dust storms in Taiwan, Environ. Res., 106, 393–400, https://doi.org/10.1016/j.envres.2007.09.006, 2008.

Chen, Q., Wang, M., Wang, Y., Zhang, L., Xue, J., Sun, H., and Mu, Z.: Rapid determination of environmentally persistent free radicals (EPFRs) in atmospheric particles with a quartz sheet-based approach using electron paramagnetic resonance (EPR) spectroscopy, Atmos. Environ., 184, 140–145, https://doi.org/10.1016/j.atmosenv.2018.04.046, 2018.

Coop, J. D., Parks, S. A., Stevens-Rumann, C. S., Ritter, S. M., Hoffman, C. M., and Varner, J. M.: Extreme fire spread events and area burned under recent and future climate in the western USA, Global Ecol. Biogeogr., 31, 1949–1959, https://doi.org/10.1111/GEB.13496, 2022.

Donahue, N. M., Robinson, A. L., and Pandis, S. N.: Atmospheric organic particulate matter: From smoke to secondary organic aerosol, Atmos. Environ., 43, 94–106, https://doi.org/10.1016/j.atmosenv.2008.09.055, 2009.

Eaton, G. R., Eaton, S. S., Barr, D. P., and Weber, R. T.: Quantitative EPR, Springer-Verlag/Wien, https://doi.org/10.1007/978-3-211-92948-3, 2010.

EPR-Interpretation: https://chem.libretexts.org/@go/page/1792, last access: 2 May 2022.

Feng, S., Gao, D., Liao, F., Zhou, F., and Wang, X.: The health effects of ambient $PM_{2.5}$ and potential mechanisms, Ecotox. Environ. Safe., 128, 67–74, https://doi.org/10.1016/j.ecoenv.2016.01.030, 2016.

Gehling, W. and Dellinger, B.: Environmentally persistent free radicals and their lifetimes in $PM_{2.5}$, Environ. Sci. Technol., 47, 8172–8178, https://doi.org/10.1021/es401767m, 2013.

Gehling, W., Khachatryan, L., and Dellinger, B.: Hydroxyl Radical Generation from Environmentally Persistent Free Radicals (EPFRs) in $PM_{2.5}$, Environ. Sci. Technol., 48, 4266–4272, https://doi.org/10.1021/es401770y, 2014.

Guo, C., Chan, T.-C., Teng, Y.-C., Lin, C., Bo, Y., Chang, L.-Y., Lau, A. K. H., Tam, T., Wong, M. C. S., and Lao, Q.: Long-term exposure to ambient fine particles and gastrointestinal cancer mortality in Taiwan: A cohort study, Environ. Int., 138, 105640, https://doi.org/10.1016/j.envint.2020.105640, 2020.

He, L., Norris, C., Cui, X., Li, Z., Barkjohn, K. K., Teng, Y., Fang, L., Lin, L., Wang, Q., Zhou, X., Hong, J., Li, F., Zhang, Y., Schauer, J. J., Black, M., Bergin, M. H., and Zhang, J.: Oral cavity response to air pollutant exposure and association with pulmonary inflammation and symptoms in asthmatic children, Environ. Res., 206, 112275, https://doi.org/10.1016/j.envres.2021.112275, 2022.

Katanoda, K., Sobue, T., Satoh, H., Tajima, K., Suzuki, T., Nakatsuka, H., Takezaki, T., Nakayama, T., Nitta, H., Tanabe, K., and Tominaga, S.: An Association Between Long-Term Exposure to Ambient Air Pollution and Mortality From Lung Cancer and Respiratory Diseases in Japan, J. Epidemiol., 21, 132–143, https://doi.org/10.2188/jea.JE20100098, 2011.

Khachatryan, L., Vejerano, E., Lomnicki, S., and Dellinger, B.: Environmentally persistent free radicals (EPFRs), 1. Generation of reactive oxygen species in aqueous solutions, Environ. Sci. Technol., 45, 8559–8566, https://doi.org/10.1021/es201309c, 2011.

Leresche, F., Salazar, J. R., Pfotenhauer, D. J., Hannigan, M. P., Majestic, B. J., and Rosario-ortiz, F. L.: Photochemical Aging of Atmospheric Particulate Matter in the Aqueous Phase, Environ. Sci. Technol., 55, 13152–13163, https://doi.org/10.1021/acs.est.1c00978, 2021.

Li, T., Wang, Z., Wang, Y., Wu, C., Liang, Y., Xia, M., Yu, C., Yun, H., Wang, W., Wang, Y., Guo, J., Herrmann, H., and Wang, T.: Chemical characteristics of cloud water and the impacts on aerosol properties at a subtropical mountain site in Hong Kong SAR, Atmos. Chem. Phys., 20, 391–407, https://doi.org/10.5194/acp-20-391-2020, 2020.

Liu, Y. and Chan, C. K.: The oxidative potential of fresh and aged elemental carbon-containing airborne particles: a review, Environ. Sci.-Proc. Imp., 24, 525–546, https://doi.org/10.1039/d1em00497b, 2022.

Majestic, B. and Runberg, H. L.: Data Set for "Atmospheric Aging of Combustion-Derived Particles: Impact on Stable Free Radical Concentration and Its Ability to Produce Reactive Oxygen Species in Aqueous Media", Digital Commons [data set], https://doi.org/10.56902/Chem.Data.2023.1, 2023.

Petrakis, L.: Spectral Line Shapes Gaussian and Lorentzian functions in magnetic resonance, J. Chem. Educ., 44, 432–436, 1967.

Runberg, H. L. and Majestic, B. J.: Hydroxyl radical (OH) formation during the photooxidation of anthracene and its oxidized derivatives, Atmos. Environ., 286, 119214, https://doi.org/10.1016/J.ATMOSENV.2022.119214, 2022.

Runberg, H. L., Mitchell, D. G., Eaton, S. S., Eaton, G. R., and Majestic, B. J.: Stability of environmentally persistent free radicals (EPFR) in atmospheric particulate matter and combustion particles, Atmos. Environ., 240, 117809, https://doi.org/10.1016/j.atmosenv.2020.117809, 2020.

Sigmund, G., Santín, C., Pignitter, M., Tepe, N., Doerr, S. H., and Hofmann, T.: Environmentally persistent free radicals are ubiquitous in wildfire charcoals and remain stable for years, Commun. Earth Environ., 2, 68, https://doi.org/10.1038/s43247-021-00138-2, 2021.

Sorin, L. A. and Vlasova, M. V.: EPR Line Shapes and Line Widths, in: Electron Spin Resonance of Paramagnetic Crys-

tals, Springer, Boston, https://doi.org/10.1007/978-1-4615-8690-6, 111–124, 1973.

Stoll, S. and Schweiger, A.: EasySpin, a comprehensive software package for spectral simulation and analysis in EPR, J. Magn. Reson., 178, 42–55, https://doi.org/10.1016/j.jmr.2005.08.013, 2006.

Tian, L., Koshland, C. P., Yano, J., Yachandra, V. K., Yu, I. T. S., Lee, S. C., and Lucas, D.: Carbon-Centered Free Radicals in Particulate Matter Emissions from Wood and Coal Combustion, Energ. Fuel., 23, 2523–2526, https://doi.org/10.1021/ef8010096, 2009.

Tong, H., Lakey, P. S. J., Arangio, A. M., Socorro, J., Shen, F., Lucas, K., Brune, W. H., Pöschl, U., and Shiraiwa, M.: Reactive Oxygen Species Formed by Secondary Organic Aerosols in Water and Surrogate Lung Fluid, Environ. Sci. Technol., 52, 11642–11651, https://doi.org/10.1021/acs.est.8b03695, 2018.

Vidrio, E., Phuah, C. H., Dillner, A. M., and Anastasio, C.: Generation of hydroxyl radicals from ambient fine particles in a surrogate lung fluid solution, Environ. Sci. Technol., 43, 922–927, https://doi.org/10.1021/es801653u, 2009.

Wang, Y., Li, S., Wang, M., Sun, H., Mu, Z., Zhang, L., Li, Y., and Chen, Q.: Source apportionment of environmentally persistent free radicals (EPFRs) in $PM_{2.5}$ over Xi'an, China, Sci. Total Environ., 689, 193–202, https://doi.org/10.1016/j.scitotenv.2019.06.424, 2019.

Wu, C., De Visscher, A., and Gates, I. D.: Reactions of hydroxyl radicals with benzoic acid and benzoate, RSC Adv, 7, 35776–35785, https://doi.org/10.1039/C7RA05488B, 2017.